International Journal of ChemTech Research
CODEN (USA): IJCRGG, ISSN: 0974-4290, ISSN(Online):2455-9555
Vol.9, No.07 pp 688-701, 2016

Defect Mediated Blue Emission and Ferromagnetism in Ni doped ZnO Nanocrystals

S. Kanchana[1], M. Sathya[2], K. Pushpanathan[2]*, Suhashini Ernest[1],

[1]PG and Research Department of Physics, Urumu Dhanalaksmi College, Tiruchirapalli-620 019, India.
[2]Nanomaterials Research Laboratory, Department of Physics, Government Arts College, Karur- 639 005, India.

Abstract : This article deals with the synthesis and characterization of nickel doped zinc oxide nanopowder prepared by precipitation method. Synthesized nanopowders were analysed for morphological, structural and optical properties. X-ray diffraction study confirmed the substitution of nickel ion without disturbing the basic wurtzite structure of zinc oxide. The average crystalline size was found to increase on nickel doping as compared to undoped zinc oxide. The lattice constants also increased with nickel content. Scanning electron microscope study also confirmed the existence of particles in nanometer size. Furthermore, scanning electron micrograph established the increase of particle size on nickel doping. Tauc's relation shows that energy gap of zinc oxide decreases with the increase of nickel content. The violet and blue emission lines of photoluminescence spectrum also deep-rooted the substitution of nickel ion in zinc oxide.
Keywords : Nanoparticle; Energy gap; Crystal structure; Microstructure; Photoluminescence.

1.Introduction

Transition metal (TM) doped zinc oxide (ZnO) nanomaterials has wrapped up enormous interest during the last few years, due to their prospective application in spintronic devices[1-10]. Spin of the electron plays a major role in reading and writing information in these spintronic devices[11]. Generally, TM doped nanomaterials are branded as diluted magnetic semiconductors (DMSs). The quiet feature of DMSs is that they possess both room temperature ferromagnetism as well as semiconducting properties. In traditional semiconducting materials *such as* Si and Ge, the electrical conduction is based on the control of electrons *or* holes. But TM doped ZnO provides a new type of controlled conduction. These magnetic semiconductors allow a control of quantum spin state (up or down) *i.e*., just by changing the spin of the electrons and it is possible to read/write information in the memory devices[12].This would theoretically provide near-total spin polarization which is an important property for spintronic applications. Besides, transition metals do not affect the band-to-band absorption spectrum of ZnO, but they strongly modify the luminescence properties[13].They don't introduce extra charge carriers, but rather provide impurity centres that interact with the quantum confined electron-hole pair. Since these impurities can be paramagnetic, they also introduce a localized spin into the nanocrystals[14]. Such doped luminescent semiconductor nanoparticles are of brawny interest for its possible use in optoelectronic devices, such as, light-emitting diodes, spin valve transistors, spin light-emitting diodes, non-volatile memory, and lasers and as novel phosphors because of their interesting magnetic[15] and optical properties[16]. Owing to these reasons, TM doped ZnO is becoming a thrust area in the field of spintronics. Among the different transition metals, like Co, Ni, Cu, Mg etc., Ni has its own significance that (i) it act as a well-known luminescence activator, which

can modify the luminescence of ZnO crystals by creating localized impurity levels, (ii) it is compatible with Zn for successful doping (iii) it can modify the morphology and optical characteristics of ZnO nanostructures[17]

Comprehensive literature survey infers that countable articles have been published on the synthesis and properties of Ni doped ZnO nanopowders. *For instance*, Khatoon and Ahmad[18], have synthesized the Ni doped ZnO nanoparticles using modified solvothermal method and investigated the optical and magnetic properties of Ni-doped ZnO nanoparticles. They found that modified solvothermal method yields nanoparticles with significantly high surface area compared to other methods. In another study, Wang *et. al.,*[19] has prepared the Ni-doped ZnO nanoparticles through ultrasonic assisted sol–gel process and studied their structure and room-temperature ferromagnetism. Likewise, the temperature induced ultraviolet emission property of the polymer capped ZnNiO system has been investigated by Shijina *et.al.,*[20] Their result shows that intensive UV emission property of the polymer capped ZnNiO seems to have a great potential for applications in fabricating nanoscale UV light emitters. The sol-gel auto-combustion method followed by Elilarassi and Chandrasekaran[21] clearly indicates the possibility for the formation of NiO secondary phase of NiO as the Ni content is 2%. However, no such secondary phases have been observed in ZnO:Ni samples till 3% doping. The crystallite size was found to increase up to 3% and then decreased for 5% Ni doping. The results of influence of TM ions on the structural and magnetic properties of ZnO thin films deposited by sol-gel method reveals that the level of doping is crucial for obtaining the magnetic properties at room temperature[22]. These literature surveys clearly indicate that only few attempt have been devoted on the synthesis of Ni doped ZnO nanoparticles by chemical route. In fact, chemical precipitation method is very attractive because it is an inexpensive, simple, trouble-free, and expedient route to get large quantities of ZnO nanoparticles. Also, we can control the morphology of the nanoparticles by controlling the rate of hydrolysis, reaction temperature, time, and concentration of precursors. Besides, precipitation method yields smaller nanoparticles than the sol-gel and hydrothermal methods. On account of these industrial values, we have chosen the chemical precipitation method for the present work.

As pointed above, even if many work have been carried out on Ni-doped ZnO system, most of them focusing on thin films and the detailed study of structural and optical properties of Ni doped ZnO nanopowders is still inadequate. Therefore, the main goal of this work is to evaluate the consequence of Ni doping on crystal structure, morphology, optical and magnetic properties of ZnO nanoparticles. Although synthesis and characterization of Ni doped ZnO nanoparticles is an incremental work, the most significant finding of the present work opens the possibility of Ni doping up to 5% in ZnO matrix without any secondary phase.

2. Experimental Procedure

2.2 Synthesis of ZnO and Ni doped ZnO nanoparticles

Nanocrystalline $Zn_{1-x}Ni_xO$ (x = 0, 0.03, 0.05) powder samples were synthesized by a simple chemical precipitation method summarized as follows. All the chemicals used here are of analytical grade and used without further refinement. The beaker and other glass wares used in this work were washed with acid. Ethanol and double distilled water were used as solvent for sample preparation. Synthesis procedure was carried out at room temperature (34˚C).

Analytical reagent chemicals zinc acetate [$Zn(CH_3COO)_2$. $2H_2O$], nickel acetate [Ni $(CH_3COO)_2$ Merck] sodium hydroxide (NaOH) and polyethylene glycol (PEG MW:400) supplied by Merck were used to synthesize undoped ZnO and Ni doped ZnO nanoparticles. Initially, 2 gm of NaOH was dissolved in the mixture of 25 ml double distilled water and 25 ml ethanol. Alternatively, xNi$(CH_3COO)_2.4H_2O$ and (1-x)$Zn(CH_3COO)_2.2H_2O$ (x = 0,0.03 and 0.05) were dissolved in the mixture of 50 ml double distilled water and 50 ml ethanol individually and stirred constantly for 20 mins to get the homogenous solution. Following this, NaOH solution was added drop by drop to the mixed solution of Ni $(CH_3COO)_2 4H_2O$ and Zn $(CH_3COO)_2.2H_2O$ and then stirred at 400 rpm for 4 hrs . The ZnO/ Ni doped ZnO dispersion in distilled water and ethanol medium was clear and transparent and the solution was kept for 20 hrs in an air tight container towards the deposition of the powder particles. In this study, transparent solution of sodium acetate Na(CH_3 COO) was removed and the particles were washed several times until the solution pH reaches 7, using double distilled water and ethanol to remove the unreacted compounds. The resulting nanocrystals were then capped with 4 ml polyethylene glycol (PEG; MW: 400). The powder thus obtained was dried at 120 ^oC for 18 hrs to remove the remaining water content from the sample. Finally, the resulting powders were annealed at 400˚C for 3hrs under air atmosphere. Complete synthesis procedure is shown in figure 1.

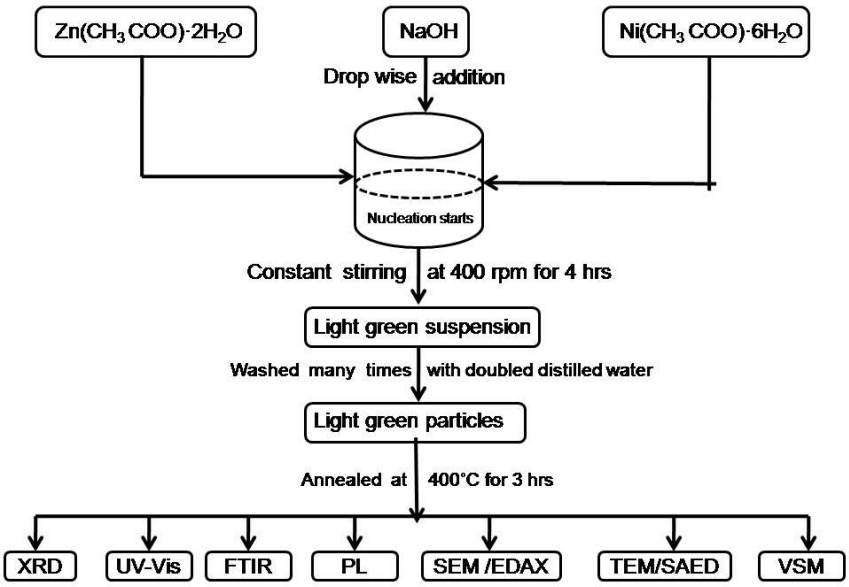

Figure 1. Synthesis process of the ZnO and ZnNiO nanopowders

2.2 Mechanism for the growth of ZnO nanoparticles

The mechanism for the growth of ZnO nanoparticles from zinc acetate dehydrate precursor can be explained as follows. Initially, zinc acetate dihydrate precursor is first dissolved in double distilled water and then hydrolyzed, which removes the intercalated acetate ions and results in zinc hydroxide solution. Then this zinc hydroxide solution transforms into Zn^{2+}cation and OH^- anion. Followed by polymerization of hydroxyl group to form Zn-O-Zn network and finally transformed into ZnO. The overall reaction can be written as;

$$Zn(CH_3COO)_2 .2H_2O + 2\ NaOH \rightarrow ZnO + 2\ Na(CH_3COO) + H_2O$$

2.3 Characterization

The crystalline nature and the phase purity of the powder samples were examined by X-ray powder diffraction (XRD) with Philips Analytical Model:X'Pert PRO equipped with Ni filtered CuKα radiation (λ = 1.54187 Å) for 2θ = 30 - 80˚, with scanning rate of 1˚/min operated at 40 kV/30 mA. Optical transmission spectra were recorded using Lambda 35 (PERKINELMER: USA) UV-Vis spectrophotometer to evaluate the energy gap. For this study, the nanopowders were dispersed in deionized water and mixed well. To identify the functional groups and to confirm the presence Ni^{2+} ions, the samples were examined with Fourier Transform Infrared Spectrometer (FTIR; RX1 PERKINELMER: USA) at a resolution of 2 cm^{-1}. The measurements were carried out in the region 400 – 4000 cm^{-1} using KBr as the beam splitter. Photoluminescence (PL) response of the powder samples was carried out by means PL spectrometer (Kimon, SPEC-14031K, Japan) with a He-Cd laser source. A line spectrum of 320 nm has been used to excite the samples. Surface morphology of the particles was examined using JEOL scanning electron microscope (JSM-6390: Japan) operated at 20kV/20mA. Chemical composition of the synthesized nanoparticles was examined by means of Energy-Dispersive X-ray Spectrometer (EDS: INCAPentaFET-x3, Oxford Instruments, UK).JEOL JEM-1010 transmission electron microscope (TEM) was used to study the microstructure and size of the nanoparticles. For TEM analysis the sample was ultrasonically dispersed in ethanol, and then a drop of a substance was placed on an amorphous carbon films supported by copper grid and dried in air. Magnetic property of the samples were experimentally studied by measuring magnetization as a function of external magnetic field at room temperature using vibrating sample magnetometer (VSM) (Lakeshore 7404).

3. Results and Discussion

3.1. Structural Characterization

The crystal structure of the ZnO / Ni doped ZnO nanoparticles; investigated by X-ray diffraction (XRD) pattern is shown in figure 2.Well pronounced sharp diffraction peaks corresponding to (1 0 0), (0 0 2), (1 0 1), (1 0 2), (1 1 0), (1 0 3), (2 0 0), (1 1 2), (2 0 1) , (004) and (002) planes were observed for all the samples. It obviously shows the crystalline nature of the nanoparticles with wurtzite structure (space group $P6_3mc$). All the peaks match well with the JCPDS data card No.79-2205. No additional peaks (such as Ni, NiO) were observed other than the above mentioned, which indicates no impurity phase exist in the samples.XRD pattern of all the samples show enhanced intensity for the peak corresponding to (101) plane.

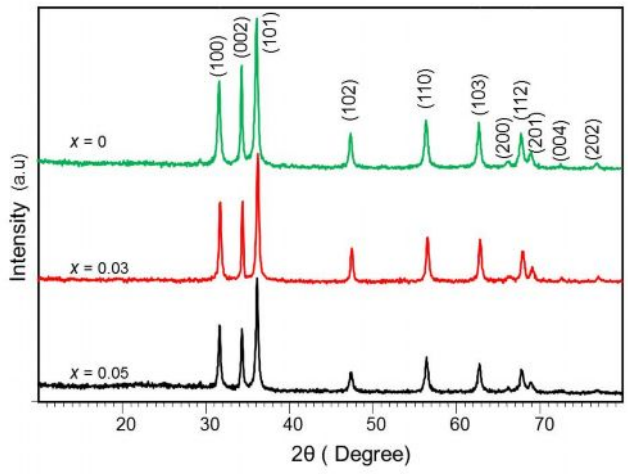

Figure 2. X-ray diffraction pattern of synthesized $Zn_{1-x}Ni_xO$ (x = 0, 0.03 and 0.05) nanoparticles.

It is noticed from the XRD pattern that the intensity of (100) and (101) peak increases whereas the intensity of (002) peak decreases, which means Ni is really doped in ZnO without disturbing the hexagonal wurtzite structure. This shows that Ni^{2+} ion replaced the Zn^{2+} available in (002) planes and the atoms available in the (101) plane is not affected. Average crystalline size D of the prepared nanoparticles has been calculated using a well-known Debye-Scherrer Formula[23].

$$D = \frac{k\lambda}{\beta_{hkl} Cos\theta}$$

where k is the shape factor (0.89 for spherical particles), λ ,is the wavelength of the CuKα radiation (0.154056 nm), and θ is the peak position. The crystalline size is 34.2nm for ZnO, 37.3nm for $Zn_{0.97}Ni_{0.03}O$, and 39.1nm for $Zn_{0.95}Ni_{0.05}O$. Calculation shows that crystalline size increases with Ni dopant which clearly reveals the presence of Ni in the prepared samples.

Table 1: Calculation Grain size, lattice constant, volume of the nanoparticle, unit cell volume, dislocation density and number of unit cell present in a grain from XRD profile.

Name of the sample	Interplanar spacing (d_{hkl})		Grain size calculated from (101) peak (nm)	Grain size from W-H method (nm)	Volume of the particle 'V' $(nm)^3$	Lattice constant		Unit cell volume 'v' $nm)^3$	Disloc..density δ x (10^{14})	No. of Unit cell present in a particle (V/ v)
	(d_{100}) plane	(d_{002}) plane				a (nm)	c (nm)			
ZnO	2.8177	2.6039	34.2	31.52	20933	0.3241	0.5186	0.04743	8.5	441345
$Zn_{0.97}Ni_{0.03}O$	2.8209	2.6047	37.3	46.23	27157	0.3252	0.5203	0.04769	4.7	569449
$Zn_{0.95}Ni_{0.05}O$	2.82079	2.6070	39.1	69.35	31281	0.3263	0.5221	0.04798	2.0	651959

The broadening of diffraction peaks evidences grain refinement along with the large strain associated with the powder samples. The instrumental broadening (β_{hkl}) is corrected, corresponding to each diffraction peak of ZnO material using the relation

$$\beta_{hkl} = \sqrt{(\beta_{hkl})^2_{Measured} - (\beta_{hkl})^2_{Instrumental}}$$

Strain-induced broadening comes into picture from crystal imperfections and distortions which are related by ε = $[(\beta]_1 s$ /tanθ). Consequence of this equation is the dependency on the diffraction angle θ. The Williamson-Hall (W-H) method does not follow (1/cosθ) dependency as in the Debye-Scherrer equation but instead varies with tanθ. This fundamental difference allows for a separation of reflection broadening when both microstructural causes- small crystallite size and micro strain occur together. The distinct θ dependencies of both effects laid the basis for the separation of size and strain broadening in the analysis of Williamson and Hall[24]. Addition of the Debye-Scherrer equation and ε = $(\beta_1 s$ /tanθ) results in the following equations:

$$\beta_{hkl} = \beta_\varepsilon + \beta_D$$

$$\beta_{hkl} = \left(\frac{k\lambda}{D\cos\theta}\right)_+ (4\varepsilon\tan\theta)$$

$$\beta_{hkl}\cos\theta = \left(\frac{k\lambda}{D}\right)_+ (4\varepsilon\sin\theta)$$

The above equation is known as Williamson and Hall equation which represents that the strain is assumed to be uniform in all crystallographic directions, thus considering the isotropic nature of the crystal, where all the material properties are independent of the direction along which they are measured. A graph is drawn with respect to 4sinθ along the x-axis and β_{hkl} cosθ along the y-axis as shown in figure 3(a-c). From the linear fit to the data, the crystalline size was estimated from the y-intercept, and the strain ε, from the slope of the fit. Crystallite size estimated from W-H method also increases similar to Debye -Scherrer equation, but the crystallite sizes are found to be larger than the Debye –Scherrer method.

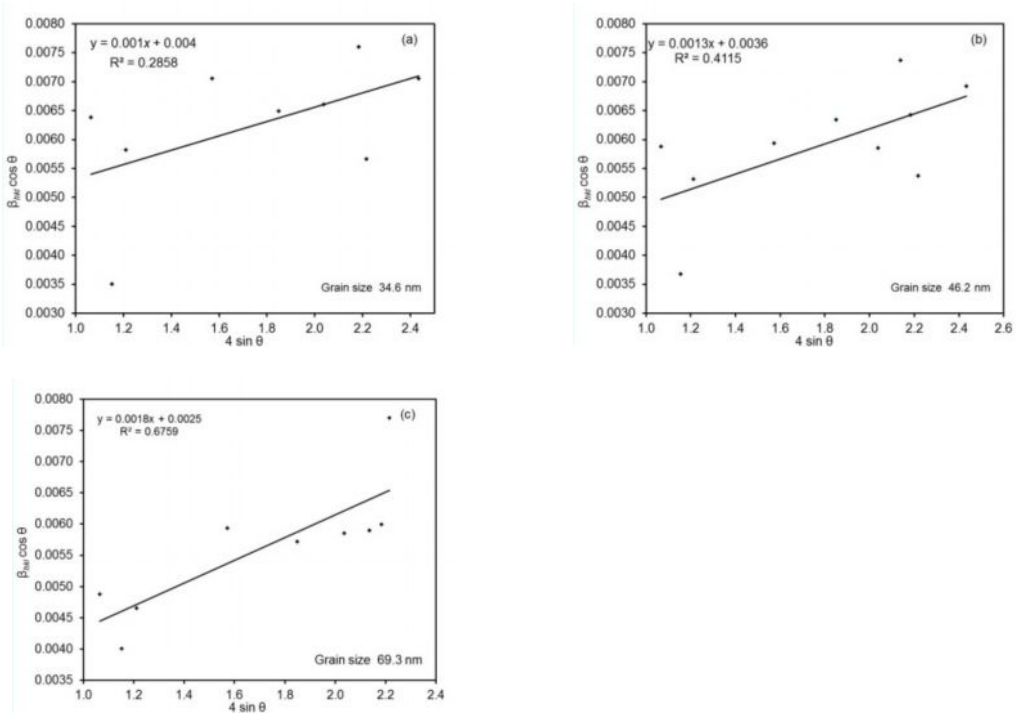

Figure 3: Williamson and Hall plot of the synthesized $Zn_{1-x}Ni_xO$ nanoparticles: (a) x = 0; (b) x = 0.03; and (c) x = 0.05.

Moreover, lattice constant 'a' and 'c' of the samples have been determined according to the following equation,

$$\frac{1}{d^2_{hkl}} = \frac{4\,(h^2 + hk + k^2)}{3a^2} + \frac{l^2}{c^2}$$

We considered (100) plane for the calculation of lattice constant '*a*'and '*c*'. Therefore, the above equation has been summarized as follows.

$a = 1.1547 \times d_{(100)}$ and 'c'$= 1.60 \times a$

Table 1 infers that the lattice constant of Ni doped ZnO are larger than that of undoped ZnO, because the ionic radius of Ni^{2+}(0.68Å) is larger than that of Zn^{2+} (0.60Å).The expansion of the lattice constants of $Zn_{1-x}Ni_xO$ indicates that nickel is really doped into the ZnO structure. The severe alteration of the lattice constant confirms the Ni doping in ZnO structure.

The dislocation density[25] δ which represents the amount of defects present in the prepared sample is determined from the formula $\delta=1/D^2$. These values are also given in Table 1. As δ is inversely proportional to D, decreasing trend of dislocation densities shows that higher concentration of Ni leads to reduce lattice imperfections. Larger value of D and smaller value of FWHM (not shown in the table) indicates better crystallization of the nanoparticles.

In order to strengthen the XRD analysis, further, the volume of the nanoparticles has been calculated from the relation $V = (4/3)\pi(D/2)^3 = 0.5233\ D^3$and the volume of ZnO:Ni unit cell has been calculated from the mathematical relation $v = (\sqrt{3}\ a^2c/2) = 0.866a^2c$. The ratio (V/ v) gives the number of unit cell present in a particle, which has been calculated from the equation 'n'$= 0.603\ (D^3/a^2c)$. Further, the Zn-O bond length (L) has been calculated by the relation,

$$L = \sqrt{0.3a^2 + (0.5 - u)^2c^2}$$

Where $u = \frac{a^2}{3c^2} + 0.25$

and it is found to be 1.8853A° for Zn-O , 1.8831A° and 1.8870 A° for$Zn_{0.97}Ni_{0.03}O$ and $Zn_{0.95}Ni_{0.05}O$, respectively. Similarly, micro-strain can also be calculated using the formula $\varepsilon = (\beta \cos\theta/4)$. It is observed that micro-strain decreased from 4.0×10^{-3} to 3.5×10^{-3} as the Ni content is increased from 0 to 5%. In general, variation in micro-strain may be due to the change in microstructure, size and shape of the particles. The atoms trapped in the non-equilibrium position could shift to a more equilibrium position, and it could release the strain. Hence, the Ni substitution decreases the micro-strain of the ZnO nanoparticles.

3.2 Energy gap determination from Tauc's plot

Effect of Ni substitution on wurtzite structure of ZnO was further examined using UV–Visible optical transmittance spectrum measured in the range 200–1100 nm which was used to draw the Tauc's plot. A Tauc's plot[26] is a graph that is used to determine the optical band gap of semiconductors. The Tauc's gap is often used to characterize practical optical properties of amorphous materials. Figure 4(a-c) shows typical Tauc's plot of undoped and nickel doped ZnO nanoparticles. In Tauc's plot, the absorption coefficient and the energy band gap is related by the following equation;

$$(\alpha h\upsilon) = A\,(h\upsilon - Eg)^{1/2}$$

where hυ is the photon energy, α is the absorption coefficient, and A is a constant. A plot of hυ versus $(\alpha h\upsilon)^2$ is drawn to determine band gap (Eg) using the linear fit process. The resulting plot has a distinct linear regime which denotes the onset of absorption. Thus, extrapolating this linear region to the abscissa yields the optical band gap of the semiconductor nanoparticle. The band gap measured to be 3.44 eV, 3.32 eV and 3.20 eV for undoped, 3% Ni doped and 5%Ni doped ZnO nanoparticles, respectively.

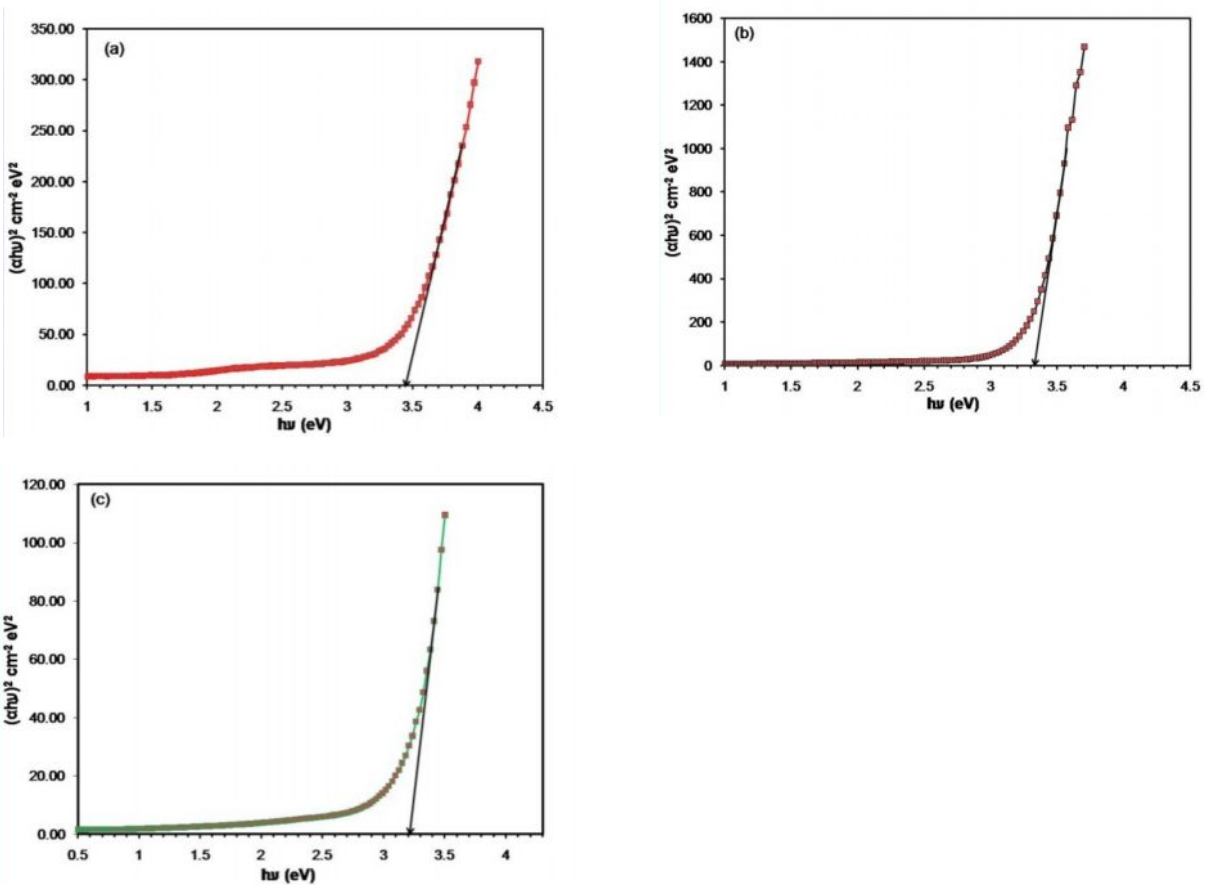

Figure 4.Tauc's plot of $Zn_{1-x}Ni_xO$ nanoparticles. (a) $x = 0$; (b) x=0.03 and (c) $x = 0.05$

3.3 FTIR Spectrum - Analysis

Figure 5 depicts the FTIR spectra of ZnO and Ni doped ZnO nanoparticles. The bands at 3440–3245 cm^{-1} correspond to the stretching vibration of O-H molecule. A strong asymmetric stretching vibration of C=O has been observed between 1648 and 1565 cm^{-1}. The peaks between 1410 and 1211cm^{-1} corresponds the symmetric stretching vibration of C-O bond. Because of similar structural morphologies in acidic conditions, both of C=O, C-O peaks were not shifted greatly. The peak cantered at 1093 cm^{-1} is caused by C–O–C functional group. No sign of NiO *or* Ni_3O_4 impurities. This is the sign of high purity of the samples and this implies that mixing of distilled water and CH_3CH_2OH gives the good result of synthesis of Ni doped ZnO from $Zn(CH_3COO)_2{\cdot}2H_2O$ precursor. Wavenumber of all the functional groups is almost same, irrespective of Ni content, except Zn-O and Zn-Ni-O groups. The ZnO peak at 499 $cm^{-1}$and Ni-doped ZnO peaks at 619 $cm^{-1}$and 651 cm^{-1}confirmed the complete transformation of zinc acetate and nickel acetate into ZnO and Ni doped ZnO, respectively. In fact, XRD and EDS analysis proved that the synthesized powders are highly pure. The Ni dopant shifted the IR peak considerably from 499 cm^{-1} to 651 cm^{-1} depending on concentration. This shift in IR peak confirmed the Ni doping. Previous researchers[27]found the ZnO peak at 464 cm^{-1}. Thus, our result confirms the previous report. The FTIR results support the SEM results.

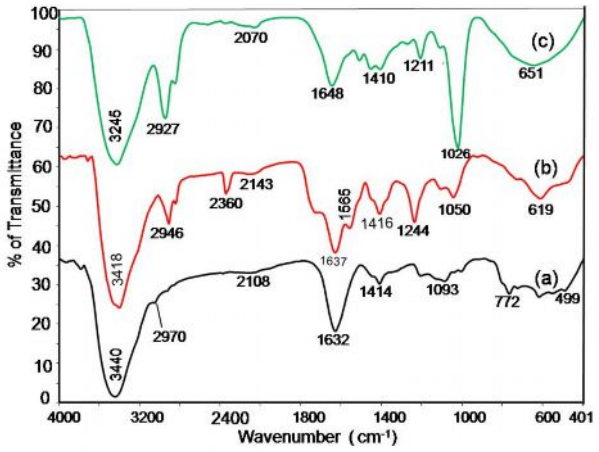

Figure 5. Typical FTIR spectrum and their peak assignments

3.4 PL Spectrum

To analyze the role of Ni content on the structural defects and the band gap of ZnO nanoparticles, photoluminescence (PL) spectra of undoped and Ni doped ZnO samples recorded at room temperature are shown in figure 6 (a-c).

It is noticed that undoped ZnO sample exhibits four emission lines. They are at the wavelength of (i) 384 nm (UV emission), (ii) 430 nm (violet emission), (iii) 485 nm (greenish –blue) and (iv) 517 -535 nm (green emission). Of these, UV and violet emissions are wide and the greenish- blue emission line is sharp and narrow. Literature survey infers that the UV emission originates from the exciton recombination corresponding to the near band edge (NBE)[28], through exciton-exciton collision. The strong violet emission band is centered at 430 nm. Origin of the violet emission from the undoped ZnO is assumed to be the recombination from the defect centers such as O and Zn interstitials. It is reasonable to consider that this type of violet emission is rarely reported. The luminescent peak centered at 485 nm is assigned to the greenish - blue excitonic emission, corresponding to the energy gap of 2.56 eV. As well, we have observed a weak green emission peak between 517–535 nm. This green emission is attributed to the transition between photo-excited holes and singly ionized oxygen vacancies[29] in ZnO and this oxygen vacancies could have been produced at the time of sample preparation. Generally, undoped ZnO emits its characteristic UV radiation. But in our case, we observed a strong violet emission. Therefore, it is believed that the undoped ZnO has more number of Zn and O interstitial defect centres.

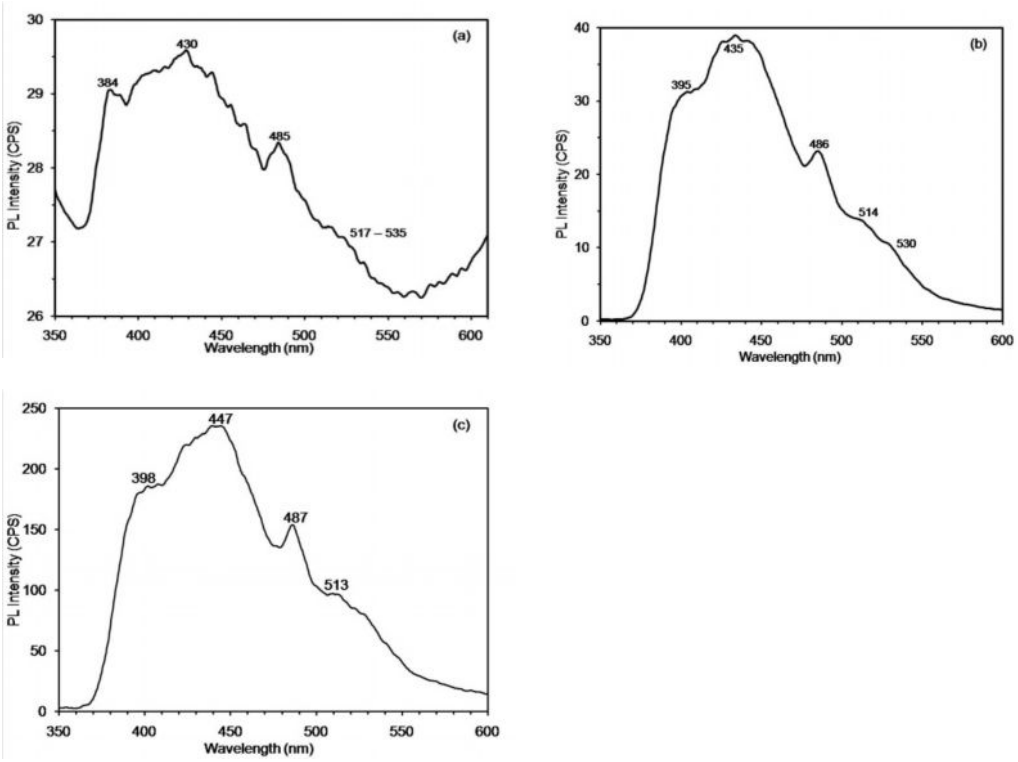

Figure 6. Photoluminescence spectra of (a) ZnO; (b) 3%Ni doped ZnO; and (c) 5% Ni doped ZnO nanoparticles.

Comparing with undoped ZnO sample, PL spectra of ZnO:Ni samples are motivating one. Particularly, UV peak is obscured and there is a little trace of UV emission. At the same time, visible emission is shifted from violet (431 nm) to blue (447 nm) as the Ni content reaches 5%. In addition, intensity of blue emission is perceptibly improved. The improvement in blue and green emissions is from the rise in oxygen vacancies, which are induced by Ni doping. Furthermore, it is noticeable that for 3% of Ni, greenish - blue emission peak around 486 nm is well sharp whereas the green emission (514-530 nm) is very pathetic (~ 513 nm). As the Ni content is increased to 5%, greenish-blue emission band shifted 487 nm. It should also be noted that the less intense green peak shifted to lower wavelength of 513 nm. This indicates that creation of oxygen vacancies is limited on 5% Ni doping.

It is interesting to note that Ni doping changes the emission property of basic ZnO matrix from violet to blue. This type of unusual photoluminescence property may be ascribed to the remarkable changes in the concentration of the defects of the Ni doped sample reported here. Moreover, the hoist in the PL intensity with Ni doping is ascribed to the decrease in non-radiative recombination process. From the photoluminescence study, it is clear that Ni doping severely suppresses the UV emission of ZnO, which is in good agreement with the results reported earlier in the literatures[30,31]. Diminish of characteristic UV emission and the shifting and enhancement of intensity of visible emission from violet to blue in (435-447 nm) confirmed the Ni substitution in ZnO nanoparticles.

3.5 SEM and EDS analysis

SEM micrographs of synthesized nanopowders of $Zn_{1-x}Ni_xO$ (x = 0.00, 0.03, and 0.05) are shown in figure 7(a–c). SEM studies show that the powders consist of highly agglomerated nanoparticles with few nanorods resulting from overlapping of small particles when annealed at 400 °C for 3 hrs. Particle size estimated using SEM micrograph is found to be lying in the range from 32 to 79 nm, for undoped and $Zn_{0.95}Ni_{0.05}O$ samples, respectively. In particular, there is no appreciable change in the morphology of ZnO, when it is doped with 5 % of Ni content. The particles size is small and distributed uniformly throughout the

entire surface. We have observed that the agglomeration increases with Ni content and this agglomeration could be attributed to their extremely small dimensions with high surface energy crystallization and drying process.

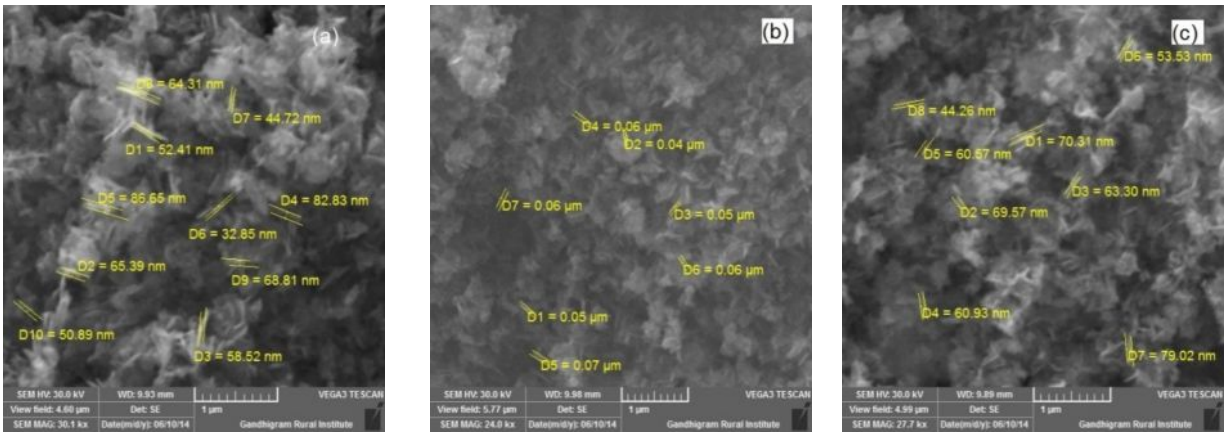

Figure 7. SEM image of prepared (a) undoped ZnO; (b) $Zn_{0.97}Ni_{0.03}O$; and (c) $Zn_{0.95}Ni_{0.05}O$ nanoparticles.

The EDS spectrum of the ZnO and $Zn_{0.97}Ni_{0.03}O$ samplesare displayed in figure 8 (a&b). The spectrum confirms the presence of nickel dopant in ZnO nanoparticles. EDS spectrum for all the three samples have been recorded, but for ZnO and $Zn_{0.97}Ni_{0.03}O$ samples only are displayed here. The spectrum shows Zn, Ni, and O related peaks. The weight ratio (x) of Ni to Zn has been determined from the relation x = Ni/ ([Zn + Ni]) and it is found to be 2.14 and 4.32 % doping. EDS analysis gives how much amount of Ni atom has really entered into the ZnO nanoparticles. We actually doped 3 and 5%Ni. But EDS spectra show that only 2.14 and 4.32% of Ni atoms has entered into the ZnO. Remaining Ni atoms should have been washed away (or) impurity should have been formed. But, we have not recorded any peak accountable for secondary phase. Therefore, it is concluded that the rest of the Ni atom could have been removed on washing. Weight percentage (wt %) shown in Table 2 proves that the ratio of Ni dopant in the samples are approximately equal to the nominal composition. Thus, composition analysis confirms the incorporation of Ni element in the samples.

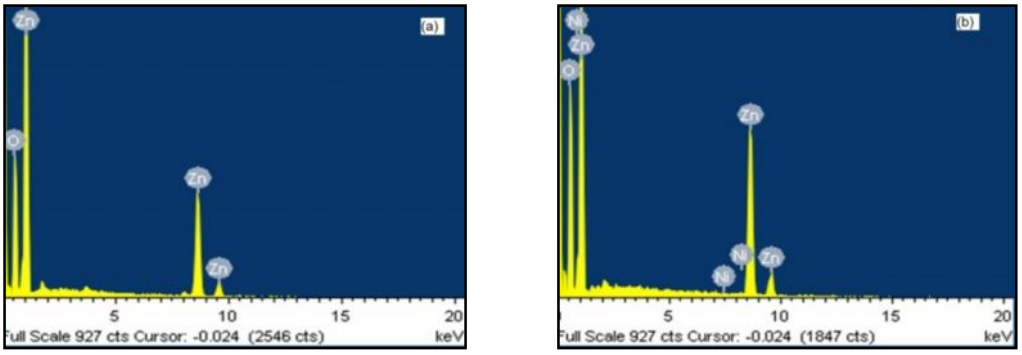

Figure 8: EDS spectrum of synthesized $Zn_{1-x}Ni_xO$ nanoparticles. (a) x = 0 and (b) x = 0.05confirms the presence of Ni, Zn and O.

Table 2. Result of elemental analysis of undoped / Ni doped ZnO nanoparticles

Elements	Composition in (wt %)		
	Undoped	Ni -3%	Ni -5%
Zn	67.64	55.50	59.65
O	32.36	42.36	36.03
Co	-	2.14	4. 32
Total	100	100	100

3.6 TEM Analysis

In order to get direct information about the particle size and morphology of the synthesized nanocrystalline samples, transmission electron micrograph analysis were made. Representative TEM image of 5% Ni doped ZnO sample and its corresponding selected area diffraction pattern (SAED) and fringe width patterns are shown in figure 9 (a-c). From the figure, it can be seen that the sample contains particles of uniform sizes.

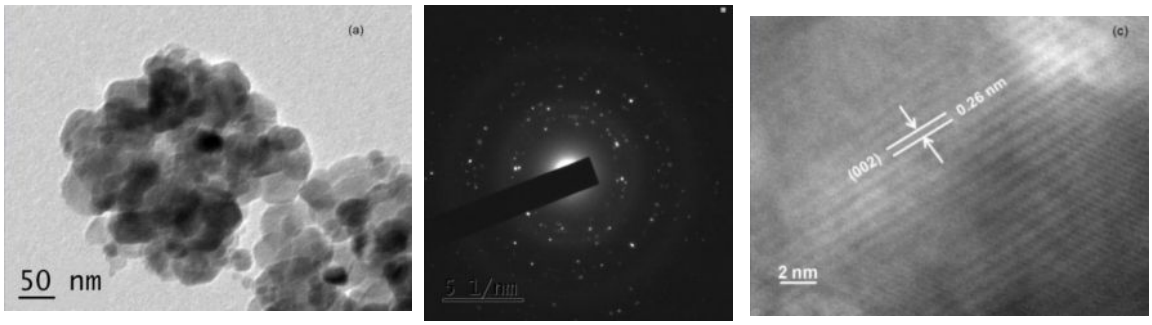

Figure 9. TEM image (a); SAED pattern (b); and fringe width pattern of the $Zn_{0.95}Ni_{0.05}$ Onanoparticles (c).

The calculated average particle size from TEM analysis is about 40-65 nm which matches well with the value obtained from W-H method. The SAED pattern indicates that the particles are single crystalline in nature and are free from major lattice defects. The fringe pattern with plane distance of 0.26 nm corresponds to (002) plane of pure wurtzite hexagonal structure of ZnO. SAED pattern reveals that the ZnO:Ni system exhibits a single crystalline structure which is in good agreement with the XRD result.

3.7 Magnetic field vs. Magnetization of $Zn_{1-x}Ni_xO$ nanoparticles

After successful synthesis and structural characterization, we precede with the magnetic measurement for the synthesized nanocrystals. Results of the magnetic field vs. magnetization (M-H) of $Zn_{1-x}Ni_xO$ (x = 0.0, 0.03, and 0.05) samples recorded at room temperature in the range of ±20 G is displayed in figure 10 and 11(a&b). Of these, figure 10 is the typical magnetic field vs. magnetization curve of undoped ZnO nanoparticles. It shows a mixed state of ferro and diamagnetic behaviour. A clear ferromagnetic hysteresis loop appeared between - 6.5G and 6.5 G is the evidence of ferromagnetic property (shown in the inset) of undoped ZnO. Magnetic field below - 6.5 G and above 6.5 G the sample shows the diamagnetic property.

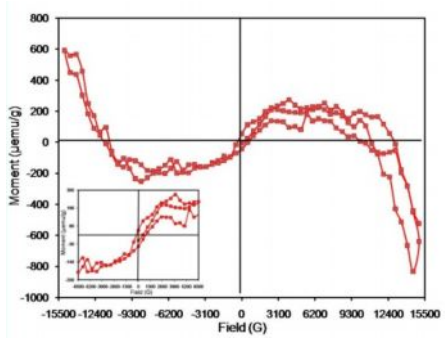

Figure 10. Magnetic field vs. Magnetization curve of undoped ZnO nanoparticles

Considerable saturation magnetization 273 μemu/g has been observed in the ferromagnetic region. This type of mixed ferro and diamagnetism has also been observed by us in our recent work[13] and by others[32, 33].In fact, origin of room temperature ferromagnetism (RTFM) in undoped ZnO is still a hot issue. Many possibilities have been proposed to give a rational elucidation for the origin of RTFM in pure ZnO. According to Sundaresan *et.al.,*[34] and Norberg[35], lattice defects is the source of RTFM in undoped ZnO nanoparticles. Likewise, Zhang *et. al.,*[36] argued that the strong interaction between the localized interstitial Zn 4*s* level and the

conduction band is the origin of ferromagnetic behaviour. In our case, we observed ferromagnetism in the lower magnetic field < ±6.5 G. We believe that the observed Zn and O interstitial defect centres (Refer *PL studies*) are responsible for this ferromagnetic property. Thus we also confirm that interstitial defect centres are responsible for the ferromagnetism in undoped ZnO nanoparticles. However, the matter of what causes the observed ferromagnetism in undoped ZnO nanoparticles is still remains open.

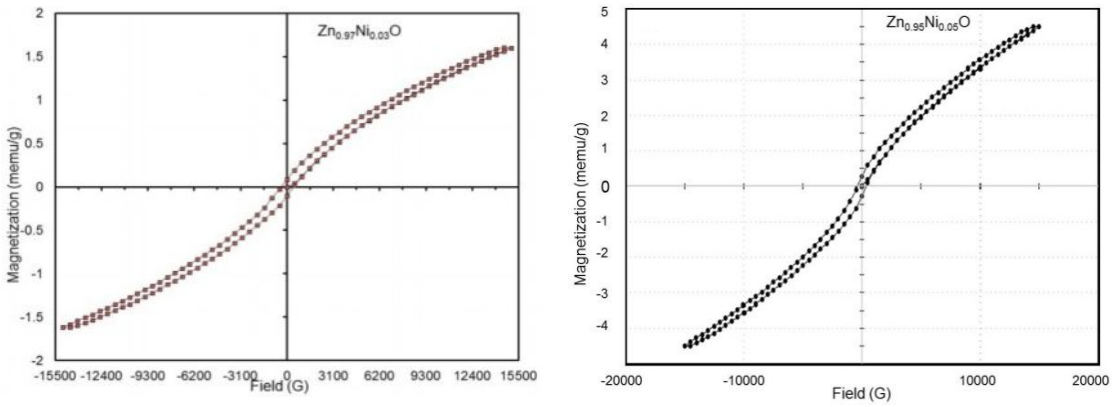

Figure 11. Magnetic field vs. Magnetization curve of $Zn_{0.97}Ni_{0.03}O$ (Left); and $Zn_{0.95}Ni_{0.05}O$ (Right) nanoparticles.

Figure 11 shows the room temperature M–H loop for the 3 and 5% Ni doped ZnO nanoparticles. The observed saturation magnetic moment (M_s) is of the order of 1.6 memu/g for 3% Ni doping and it enhanced nearly 3 times (4.6 memu/g) on 5% Ni doping. For practical applications, the transition temperature (T_c) of the TM doped ZnO nanoparticle should be well above room temperature. It is clear from the M–H loop presented here that the reported Ni doped ZnO nanoparticles can retain ferromagnetic nature up to far above room temperature. Note that the observed M_s value is increasing with increasing Ni content. As more ferromagnetic Ni ions are incorporated inside the ZnO matrix for 5% of Ni doping, as a result the overall magnetic moment has increased. At the same time magnetic moment didn't attains the saturation, i.e., still increases even beyond ±15,500 G. The increase in magnetic moment indicates that the observed ferromagnetic interaction is from substituted Ni ions. It is believed that more and more Ni ions generates antiferromagnetic order over ferromagnetic and this will restrict the nanoparticles attaining saturation magnetization.

4. Conclusions

In conclusion, we have successfully synthesized the undoped ZnO and Ni doped ZnO nanopowders by simple precipitation method. XRD pattern confirmed that the samples contain the nanoparticles of size ~34 – 39 nm whereas the W-H method confirmed that the size of the particles are 34.6 – 69.3 nm. Tauc's relation concludes Ni doping reduces the energy gap of ZnO greatly to 3.20 eV on 5% doping. The average particle size measured from SEM analysis is 40 - 80 nm which is nearly equal to the grain size measurement by W-H method. EDS analysis of the prepared ZnO /Ni doped ZnO nanoparticles confirmed that the samples are composed of Zn, Ni and O without any other impurity. FTIR spectra confirmed the Ni substitution through the shift of IR peak from 499 cm^{-1} to 651 cm^{-1}. PL studies confirmed that the ZnO samples contains Zn and O interstitial defect which induces the violet emission. PL study also concludes that Ni substitution diminishes the UV emission and enhances the blue emission. Based on the result presented here, it is concluded that the precipitation method is a competent method for the synthesis of Ni doped ZnO nanoparticles without any impurity phase and the Ni doped ZnO nanoparticles can be used for the construction for the blue colour emitting optoelectronic devices.

Acknowledgement

Authors thank SAIF IIT(M) for providing TG and DSC analysis and STIC – Cochin for providing TEM experimental facilities to carry out the present work. One of the authors (SK) also thank Research Scholars M.JayChithra, C.Thangamani and M.Ponnar of Nanomaterials Research Laboratory, Department of Physics, Government Arts College, Karur - for their timely help in the synthesis process.

References

1. Pan F, Song C, Liu XJ, Yang YC, Zeng F. Ferromagnetism and possible application in spintronics of transition-metal-doped ZnO films. Mater. Sci. Eng., R, 2008,62; 1–35.
2. Vijayaprasath G , Murugan R, Ravi G. Structural, Optical and Magnetic Properties of Ni Doped ZnO Nanostructures Prepared by Co-Precipitation Method. ;International Journal of ChemTech Research, 2014, 6; 3385-3387.
3. Nithya R, Kannan AG , Manjulavalli TE. Investigation of Pure and Transition Metal Doped ZnO Nanoparticles for Photovoltaic Applications. ;International Journal of ChemTech Research, 2014-2015, 7; 1178-1184.
4. Tamil Illakkiya J, Hemalatha S, Oommen R, Usha Rajalakshmi P. Characterization of ZnO Nanoparticles synthesized by wet chemical method; International Journal of ChemTech Research, 2014, 6; 2159-2161.
5. Sugapriya S , Lakshmi S , Senthilkumaran CK. Effect on Annealing Temperature on Zno Nanoparticles. ;International Journal of ChemTech Research, 2015, 8; 297-302.
6. Thamima M, Karuppuchamy S. Microwave Assisted Synthesis of Zinc Oxide Nanoparticles, ;International Journal of ChemTech Research, 2015, 8; 250-256.
7. Panchavarnam D, Menaka S, Anitha A, Arulmozhi M. A Comparative Study on the Properties of ZnO and ZnS Nanoparticles ;International Journal of ChemTech Research, 2016, 9; 308-315.
8. Bomila R, Srinivasan S. Synthesis and Characterization of ZnO Nanoparticles by Wet Chemical Method, ;International Journal of ChemTech Research, 2015, 7; 3109-3114.
9. Sherly ED, Judith Vijaya J. Visible light induced photocatalytic degradation of 2,4- dichlorophenol on ZnO-NiO coupled metal oxides, ;International Journal of ChemTech Research, 2014-2015, 7; 1369-1376.
10. Pushpanathan K, Sathya S, Jay Chithra M, Gowthami S, Santhi R. Influence of Reaction Temperature on Crystal Structure and Band Gap of ZnO Nanoparticles. Mater. Manuf. Processes.,2012, *27*; 1334-1342.
11. Pearton SJ, Norton DP,Heo YW , Tien LC,Ivill MP, Li Y, Kang BS, Ren F, Kelly J,Hebard AF.ZnO Spintronics and Nanowire Devices, J. Electronic Materials.,2006, 35; 862-868.
12. Muhammad NM, Duraisamy N, Rahman K, Dang HW, Jo J, Choi KH. Fabrication of printed memory device having zinc-oxide active nano-layer and investigation of resistive switching, Curr. Appl. Phys., 2013, 13; 90–96.
13. Kanchana S, JayChithra M, Ernest S, Pushpanathan K. Violet emission from Fe doped ZnO nanoparticles synthesized by precipitation method, J. Lumin., 2016,176; 6–14.
14. Schimpf AM, Rinehart JD, Ochsenbein ST, and Gamelin DR. Charge-State Control of Mn^{2+} Spin Relaxation Dynamics in Colloidal n-Type $Zn_{1-x}Mn_xO$ Nanocrystals, J. Phys. Chem. Lett., 2015, 6; 1748−1753.
15. Choi YS. KangJW ; Hwang DK; Park SJ. Recent Advances in ZnO-Based Light-Emitting Diodes, IEEE Trans. Electron. Devices.,2009, 57; 26 – 41.
16. Jansen R, Van'tErve OMJ, Kim SD, Vlutters R, Anil Kumar PS,Lodder JC. The spin-valve transistor: Fabrication, characterization, and Physics, J. Appl. Phys., 2001, 89; 7431.
17. Khranovskyy V, Tsiaoussis I, Eriksson M,Yakimova R, Effect of Ag doping on the microstructure and photoluminescence of ZnO nanostructures, Physica Status Solidi (a) Appl. Mater. Sci.,2014, 9; 2109-2114.
18. Khatoon S and Ahmad T, Synthesis, Optical and Magnetic Properties of Ni-Doped ZnO Nanoparticles, J. Mater. Sci.Engg. B., 2012, 2; 325-333.
19. Huang GJ, Wang JB, Zhong XL, ZhouGC,Yan HL, Synthesis, structure, and room-temperature ferromagnetism of Ni-doped ZnO nanoparticles, J Mater. Sci., 2007, 42; 6464–6468.
20. Shijina K, Megha U, Varghese G. Ultraviolet multi-peak emissions of mono-dispersed polymer capped ZnNiO Nanocomposites, J.Lumin., 2014, 145; 219–223.
21. Elilarassi R, Chandrasekaran G. Synthesis, Structural and Magnetic Characterization of Ni-Doped ZnO Diluted Magnetic Semiconductor, Am. J. Mater. Sci., 2012, 2; 46-50.
22. Neamtu J, Volmer M, The Influence of Doping with Transition Metal Ions on the Structure and Magnetic Properties of Zinc Oxide Thin Films, Sci. World. J. 2014, Article ID 265969, 7 pages.
23. Patterson, A. (1939). "The Scherrer Formula for X-Ray Particle Size Determination". Phys. Rev. 56 (10): 978–982

24. Williamson GK, Hall WH. X-ray line broadening from filed Aluminium and Wolfram, ActaMetallurgica., 1953, 1; 22-31.
25. Kebbab Z, Medles M, Miloua F, Miloua R, Chiker F, Benramdane N. Experimental study on structural and optical properties prepared by spray pyrolysis technique, Physica B., 2001, 296; 319–325.
26. Tauc, J. (1968). "Optical properties and electronic structure of amorphous Ge and Si". Materials Research Bulletin 3: 37–46
27. Yuan L, Dierre B, Wang JB, Zhang BP, SekiguchiT. Spatial distribution of impurities in ZnO nanotubes characterized by cathodoluminescence, J. Nanosci.Nanotech., 2007, 7; 3323–3327.
28. Li P, Wang S, Li J, Wei Y, Structural and optical properties of Co doped ZnO nanocrystals prepared by a one-step solution route, J.Lumin. 2012, 132;220–225.
29. Udayakumar S, Renuka V, Kavitha K, Structural, optical and thermal studies of cobalt doped hexagonal ZnO by simple chemical precipitation method. J. Chem. Pharm. Res., 2012,4; 1271–1280.
30. Balti I, Mezni A,Omrani AD, Leone P, Viana B, Brinza O, Smiri LS, JouiniN.Comparative study of Ni and Co-substituted ZnO nanoparticles: Synthesis, optical, and magnetic properties, J. Phys.Che. C; 2011, 115; 15758–15766.
31. Glaspell G, Dutta P,Manivannan A, A room-temperature and microwave synthesis of M-doped ZnO (M=Co, Cr, Fe, Co & Ni)., J. Cluster Sci. 2005, 16; 523–536.
32. Zhou S, Potzger K, Reuther H, Kuepper K, Skorupa W, Helm M, Fassbender J, Absence of ferro magnetism in V-implanted ZnO single crystals. J. Appl. Phys. 2007, 101;09H109.
33. Vijayaprasath G, Murugan R, Ravi G, Structural, Optical and Magnetic Properties of Ni Doped ZnO Nanostructures Prepared by Co-Precipitation Method, ;International Journal of ChemTech Research, 2014, 6; 3385-3387.
34. Sundaresan A, Bhargavi R, Rangarajan N, Siddesh U, Rao CNR. Ferromagnetism as a Universal feature of nanoparticles of the otherwise nonmagnetic oxides., Phys. Rev.B., 2006, 74; 161306(R).
35. Norberg NS,Gamelin DR, Influence of surface modification on the luminescence of colloidal ZnO nanocrystals., J. Phys. Chem. B., 2005, 109; 20810–20816.
36. Zhang X, Zhang W, Zhang X, Xu X, Meng F, Tang CC, Defects Induced Room Temperature Ferromagnetism in ZnO Thin Films.Adv. Conden. Mat. Phys.,2014, 806327.

*****